Proceedings of the 2009 IEEE
International Conference on Information and Automation
June 22 -25, 2009, Zhuhai/Macau, China

An Improved Self-Powered Switching Interface for Piezoelectric Energy Harvesting

Junrui Liang and Wei-Hsin Liao
Department of Mechanical and Automation Engineering
The Chinese University of Hong Kong
Shatin, N. T., Hong Kong, China
Emails: {jrliang, whliao}@cuhk.edu.hk

***Abstract*— In piezoelectric energy harvesting (PEH), with the use of the nonlinear technique named *synchronized switching harvesting on inductor* (SSHI), the harvesting efficiency can be greatly enhanced. Furthermore, the introduction of its self-powered feature makes this technique more applicable for stand-alone systems. In this article, a modified circuitry and an improved analysis for self-powered SSHI are proposed. With the modified circuitry, direct peak detection and better isolation among different units within the circuit can be achieved, both of which result in further removal on dissipative components. In the improved analysis, details in open circuit voltage, switching phase lag, and voltage inversion factor are discussed, all of which lead to a better understanding to the working principle of the self-powered SSHI. Both analyses and experiments show that, in terms of harvesting power, the higher the excitation level, the closer between self-powered and ideal SSHI; at the same time, the more beneficial the adoption of self-powered SSHI treatment in piezoelectric energy harvesting, compared to the standard energy harvesting (SEH) technique.**

I. Introduction

Structured by a certain number of spatially distributed autonomous sensor devices, the wireless sensor networks (WSNs) have been widely used in military, industrial and civilian applications for monitoring different physical and environmental conditions. Many concerns on energy consumption were addressed due to their nature on wireless connections [1]. Different energy harvesting techniques have been investigated for the purpose to broaden energy sources, alleviate the dependance on batteries, and hopefully someday make all WSN devices self-powered [2].

Piezoelectric energy harvesting (PEH) is one of the promising techniques that can scavenge energy from ambient vibration sources. With its electromechanical coupling characteristic, a piezoelectric element can generate electricity when strain is produced. Since the deformation in vibrating structures is alternating, the generated electricity is also alternating. An interface circuitry is needed for AC-DC conversion. The standard energy harvesting (SEH) interface involves only a bridge rectifier for the AC-DC conversion [3], [4].

To further enhance the energy harvesting capability, Guyomar et al. proposed a nonlinear treatment named *synchronized switching harvesting on inductor* (SSHI) [5]. It was claimed that, under the same displacement excitation, SSHI can increase the harvested power by several hundred percents, compared to SEH [5], [6]. To implement SSHI, a displacement sensor and a controller were usually needed for synchronization and generation of switching commands [5]–[7], until the emergence of its self-powered version. Based on their experiment, Lallart and Guyomar claimed that the self-powered SSHI can harvest 1.6 times more of power than SEH [8]. They have also considered the influence of voltage gaps, which are produced by diodes and transistors in the circuitry, over the harvested power. Yet, the influences of other components, e.g. the capacitance of the envelope detector, have not been pointed out. Besides, two important parameters, i.e. the switching delay phase φ and inversion factor γ were regarded as constants [8]. But in fact, these two parameters are constants only when the open circuit voltage V_{OC} (related to maximum displacement) and storage voltage V_{DC} (voltage across C_{rect}) are constants. A more complete analysis should take these into account, in order to compare the energy harvesting efficiencies under different V_{OC} and V_{DC}.

In this article, the working principles of piezoelectric energy harvesting with SSHI interface are introduced in Section II. A modified circuit topology for self-powered SSHI is proposed in Section III. With the adoption of complementary topology, the peak detection unit can be separated from the switching inductive shunt; therefore, better isolation can be achieved. In Section IV, referring to the analysis in [8], an improved analysis to the self-powered SSHI is proposed. It provides a more comprehensive understanding to the self-powered SSHI. Experiments are conducted; experimental and analytical results are compared and discussed in Section V. At the end, a conclusion is given in Section VI.

II. Principles

A. Piezoelectric Energy Harvesting

Given a typical piezoelectric device, e.g. a piezoelectric cantilever with shunt circuit, its schematic representation is shown in Fig. 1(a). Under harmonic displacement excitation, the piezoelectric element can be modeled as a equivalent current source i_{eq} in parallel with the piezoelectric clamped capacitance C_p, as shown in Fig. 1(b). i_{eq} is proportional to the velocity $\dot{x}$ with the relation of

$$i_{eq}(t) = \alpha_e \dot{x}(t)\,, \tag{1}$$

where α_e is the piezoelectric force-voltage coupling factor.

978-1-4244-3608-8/09/$25.00 © 2009 IEEE.

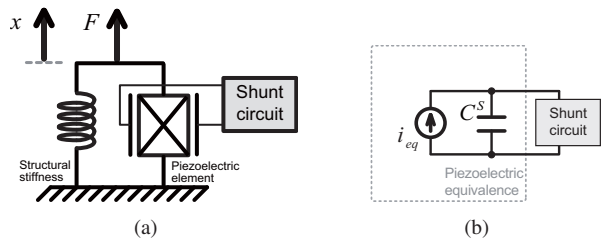

Fig. 1. Schematic representation and equivalent circuit of a typical piezoelectric device. (a) Schematic representation. (b) Equivalent circuit.

Different shunt circuits for different treatments are designed to extract energy from the vibrating mechanical structure. For the purpose of structural damping, the extracted energy is directly dissipated; while for energy harvesting, a portion of the extracted energy is reclaimed and stored in electrical form for subsequent usage.

B. SSHI

In a vibrating piezoelectric device, since the induced voltage across the piezoelectric capacitance is alternating, the most conventional way to turn an AC voltage into DC is to use a bridge rectifier for rectification and then a capacitor for filtering. The combination of bridge rectifier and filter capacitor forms the standard interface circuit that can be used for energy harvesting, i.e. SEH. Ottman et al. discussed the optimization to the SEH technique [3], [4]. Yet, using SEH cannot ensure the energy is always flowing from mechanical part to electrical part. During a certain interval in every cycle, energy returns from electrical part to mechanical part. It was called *energy return phenomenon* [9].

The SSHI treatment overcomes this problem by adding an inductive switching path to the SEH circuit. This path can be connected in parallel to the bridge rectifier to form a p-SSHI circuit (Fig. 2(a)), or in series to form a s-SSHI circuit (Fig. 2(b)) [6]. Regardless of p-SSHI or s-SSHI, the inductive switching path switches on to form a series LCR loop once the displacement x reaches its extreme values, and then switches off after half of a LCR cycle, as shown in Fig. 3(c), so as to allow a natural inversion to v_p, the voltage across the piezoelectric element. Typical waveforms of p-SSHI or s-SSHI are shown in Fig. 3. Since i_{eq} is proportional to $\dot{x}$, these switching actions make v_p in phase with i_{eq}.

To implement SSHI, additional units for displacement peak detection and switch control are required. In most of the researches, these functions were realized with displacement sensors and digital controllers [5]–[7], all of which need external power to run. In [8], all these units were replaced by a self-powered SSHI circuitry. It makes use of the piezoelectric element itself as a displacement sensor and generates switching commands with transistors accordingly. The introduction of this self-powered SSHI[1] allows the SSHI technique to be more compact and independent of external power, therefore opens a more promising future to the SSHI technique.

[1]More exactly speaking, it is a self-powered series-SSHI device.

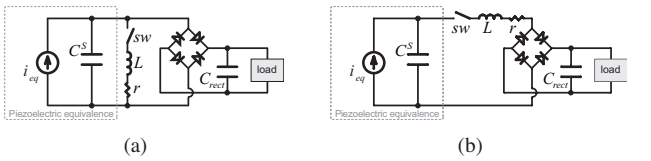

Fig. 2. Equivalent circuits of two SSHI treatments. (a) p-SSHI. (b) s-SSHI.

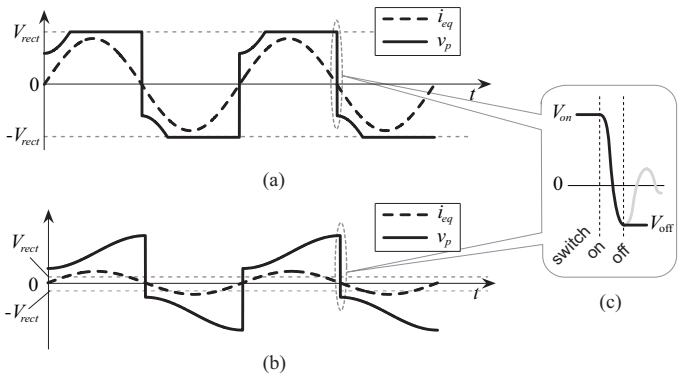

Fig. 3. Typical waveforms of two SSHI treatments. (a) p-SSHI. (b) s-SSHI. (c) Inversion of v_p at the instant of extreme displacements.

Yet, some concerns about the self-powered SSHI are still unanswered in [8], e.g., is there any constraint or applicable range for this treatment? Does the self-powered SSHI always outperform SEH? In the following sections, the self-powered SSHI treatment will be further investigated concerning these questions.

III. Circuitry

The essence of the self-powered SSHI technique proposed in [8] is the electronic breaker, which can automatically perform switching action without providing external power when the potential difference across the switch reaches its maximum. Since one breaker can only allow current flow in one direction, replacing the switch *sw* in Fig. 2 with two of such breakers (one as maximum breaker and the other, which was inversely connected, as minimum breaker), the self-powered SSHI can be achieved. The breaker consists of three parts: envelope detector, comparator, and switch. In their design, the envelope detectors are in series with the clamped capacitance C_p and inductor L. The detected voltage in fact is not v_p, but the voltage sum of v_p and the voltage across L. Even L is connected to C_p for a very short interval in every cycle, the hard switching-off action introduces high frequency components to L. The local maxima or minima produced by these high frequency components may induce misjudgement to the other breaker. Therefore, both envelope detector and comparator parts should be carefully isolated from the switching path. For the breaker introduced in [8], two resistors were connected for isolation purpose. Yet, the principle and design guideline were not clearly addressed.

Taking these envelope detection and isolation issues into consideration, in our self-powered design, we use a complementary transistors topology to achieve both direct envelope

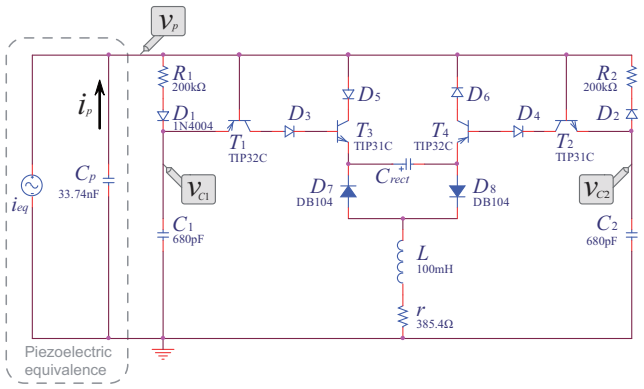

Fig. 4. Modified self-powered SSHI circuitry.

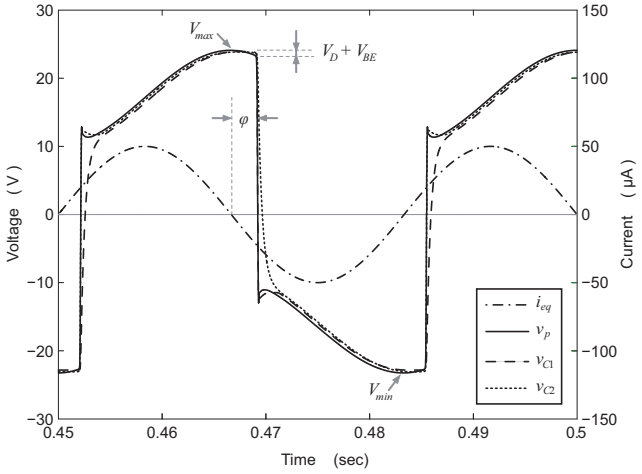

Fig. 5. Simulation waveforms in modified self-powered SSHI.

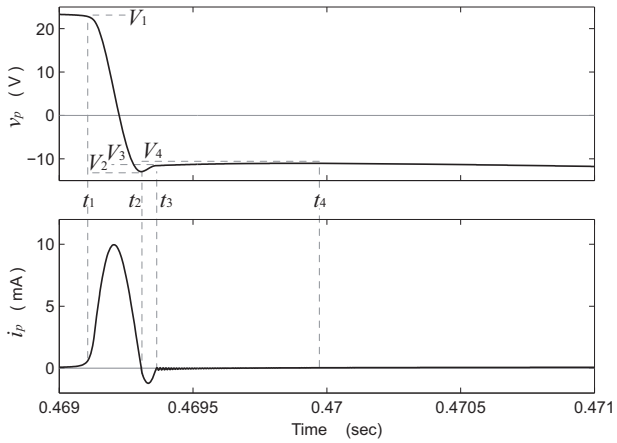

Fig. 6. v_p and i_p waveforms in the process of switching on maximum.

detection for v_p and reduction on the interference among different parts in the breakers. With this reformation, all isolating resistors, which are bound to consume some energy, can be removed. The modified circuitry is shown in Fig. 4. We obtain its waveforms (Fig. 5), as well as the zoom in view to one of the processes of switching on maximum (Fig. 6) with PSpice simulation. The part values and models given in Fig. 4 are also corresponding to those in the experimental circuit introduced in Section V[2].

For switching on maximum, R_1, D_1 and C_1 form an envelope detector. T_1 and T_3 are cut off most of the time in a cycle. When v_p reaches its maximum V_{max}, the voltage across C_1 is $V_{max}-V_D$, where V_D denotes the forward voltage drop of a diode. Then v_p begins to drop. When the decrease reaches V_D+V_{BE}, i.e. $v_p = V_1$ (t_1 instant in Fig. 6), T_1 conducts[3]. C_1 begins to discharge through $T_{1(ec)}$, D_3, $T_{3(be)}$, C_{rect}, D_8, L and r, consequently makes T_3 conduct[4]. The conduction of T_3 switches on the inductive path that consists of D_5, $T_{3(ce)}$, C_{rect}, D_8, L and r, producing a shortcut to the charge in C_p and C_2 (through D_2, R_2). For C_p, it starts a quick discharge from the voltage of V_1 through the LCR loop, until v_p reaches its local minimum V_2 (t_2 instant in Fig. 6). The current through L now tends to reverse its flowing direction, but the $T_{3(ce)}$ path is immediately blocked by reverse D_5. Yet, the path consists of D_7, C_{rect}, $T_{4(ec)}$, D_6 is still available. Because even T_4 is cut off, there is a small parasitic capacitance across its emitter and collector, which is uncharged. The current will stop flowing until T_4's emitter-collector capacitance C_{CE} is charged, at which very instant v_p becomes V_3 (t_3 instant in Fig. 6). This local minimum of v_p, i.e. V_2, may induce misjudgement for the minimum breaker. So R_2 is necessary for making sure that C_2, which is used for minimum detection, discharges slower than C_p, so as to skip over this local minimum. After t_3, both T_3 and T_4 are cut off; however, C_2 still has not finished its discharging, the rest of the charge in C_2 will flow into C_p and C_1 until they are the same in voltage. This charge neutralization again increases v_p a little bit to V_4 (t_4 instant in Fig. 6) before v_p enters the following half cycle of minimum detection.

Switching on minimum makes use of the counterparts in the circuitry, and its principle is similar to that of switching on maximum.

IV. Analysis

In Section III, the working principle of the modified self-powered SSHI circuitry has been introduced. Based on this, detailed and quantitative analysis is provided in this Section.

A. Open Circuit Voltage

Regardless of switching on maximum or minimum, the current through C_{rect} is always positive, so C_{rect} acts as energy storage. On the contrary, the average power to C_1 and C_2 is zero. They never sustain energy in themselves, so it is unsuitable to regard them as energy storage as did in [8]. Rather, C_1 and C_2 can be equivalently regarded as two capacitors connected in parallel to C_p. This approximation is validated from Fig. 5, since both v_{C1} and v_{C2} are very close to v_p. Given the harmonic displacement excitation as

$$x(t) = X\sin(\omega t), \tag{2}$$

[2]Because of the difference between the simulation models and real parts, in simulation, to properly start up the switching processes, C_1 and C_2 are set to be 2nF.

[3]V_{BE} denotes the transistor base-emitter threshold voltage.

[4]r is the equivalent series resistance of L.

where X is the amplitude of maximum displacement, ω is the vibration circular frequency. With (1), the equivalent current source should be

$$i_{eq}(t) = \alpha_e X \omega \cos(\omega t)\,. \tag{3}$$

With the parallel connections of C_p, C_1 and C_2, at open circuit condition, v_p becomes

$$v_{p,oc}(t) = V_{OC} \sin(\omega t)\,, \tag{4}$$

where

$$V_{OC} = \frac{\alpha_e X}{C_p + 2C_{ed}} \tag{5}$$

is the open circuit voltage, representing the amplitude of $v_{p,oc}$. Because the capacitances of envelope detecting capacitors C_1 and C_2 are selected to be the same, they are denoted as C_{ed} in (5). Without shunt circuit connected, the open circuit voltage of the original piezoelectric element is

$$V_{OC,org} = \frac{\alpha_e X}{C_p}\,. \tag{6}$$

Therefore, (5) implies that the open circuit voltage in self-powered SSHI will be slightly reduced under the same excitation.

In addition, to effectively drive the switches, there is a constraint for V_{OC}, which is set by the forward voltage gaps of diodes and transistors in the circuit. To figure out the constraint, suppose no any switching action is performed before the connection of the circuit. Once it is connected, the first switching action may start after v_p attains, for example, its maximum, i.e. V_{OC}, and then drop to $V_{OC} - V_D - V_{BE}$. At this time, T_1 will conduct only when v_{C1} is larger than the voltage gap produced by $T_{1(ec)}$, D_3, $T_{3(be)}$, C_{rect}, D_8 in series; and T_3 will conduct only when v_p is larger than the voltage gap produced by D_5, $T_{3(ce)}$, C_{rect}, D_8 in series. Both yield the same constraint for V_{OC} as

$$V_{OC} > V_{CE(sat)} + 3V_D + V_{BE} + V_{DC}\,, \tag{7}$$

where $V_{CE(sat)}$ is the collector-emitter saturation voltage of corresponding transistors, V_{DC} is the rectified voltage, i.e., the voltage across C_{rect}.

On the other hand, given a V_{OC} satisfying (7), we can obtain the maximum attainable V_{DC} in energy harvesting from (7), as follows:

$$V_{DC,max} = V_{OC} - V_{CE(sat)} - 3V_D - V_{BE}\,. \tag{8}$$

B. Switching Phase Lag

From the principle of SSHI [6], the switching actions should be taken at the right instants when v_p attains its extreme values, i.e. V_{max} or V_{min} in Fig. 5. In self-powered SSHI, however, to switch at the very instants is impossible; due to the voltage gaps of diode and transistor in envelope detector and comparator, there is always a phase lag between the instants of switching action start and maximum displacement (also $i_{eq} = 0$). The phase lag was defined as φ and regarded as constant in [8]. Nevertheless, φ in fact changes with V_{OC}, with the relation of

$$\varphi = \cos^{-1}\left(1 - \frac{V_D + V_{BE}}{V_{OC}}\right). \tag{9}$$

Considering the constraint on V_{OC} given in (7), the range of φ can be obtained as

$$0 < \varphi < \cos^{-1}\left[\frac{V_{CE(sat)} + 2V_D + V_{DC}}{V_{CE(sat)} + 3V_D + V_{BE} + V_{DC}}\right]. \tag{10}$$

The lower limit corresponds to infinite V_{OC}; the upper one corresponds to minimum harvestable V_{OC}.

C. Voltage Inversion Factor

The voltage inversion factor γ is an important parameter in SSHI. It makes use of the natural oscillation of a LCR circuit, so as to perform a quick inversion for v_p at right instants. During an inversion, the switch is first closed to enable a LCR loop, and then naturally blocked again after half of a LCR cycle, i.e.

$$\tau = \pi\sqrt{LC}\,, \tag{11}$$

so that the voltage across the capacitance changes at a short interval τ, which is much smaller than the mechanical cycle, with the factor of

$$\gamma = -e^{-\pi/(2Q)}\,. \tag{12}$$

This definition on voltage inversion factor [9] includes the sign information, therefore is more general, compared to that given in [8].

As described in Section III and illustrated in Fig. 6, the switching process in self-powered SSHI is more complex than that in ordinary SSHI. It might go through two inversion steps and one charge neutralization before the voltage changes from V_1 to V_4. Among these three steps, there are two intermediate values, which were denominated as V_2 and V_3 in Fig. 6. Taking switching on maximum as example, if $V_1 > V_{ref1}$, where

$$V_{ref1} = V_{CE(sat)} + 2V_D + V_{DC} \tag{13}$$

is the first reference voltage gap, v_p will experience the first inversion. For the first inversion, i.e. from V_1 to V_2, $C_p + C_1$, L and r form the LCR loop for discharging, with the quality factor of

$$Q_1 = \frac{1}{r}\sqrt{\frac{L}{C_p + C_{ed}}}\,. \tag{14}$$

The relation between V_2 and V_1 can be obtained as

$$V_2 - V_{ref1} = \gamma_1(V_1 - V_{ref1}), \tag{15}$$

where

$$\gamma_1 = \begin{cases} -e^{-\pi/(2Q_1)}, & V_1 > V_{ref1}\,; \\ 1\,, & \text{others} \end{cases} \tag{16}$$

is the inversion factor for the $C_p + C_1$, L and r loop, whose quality factor is Q_1.

After the first inversion, if $V_2 < V_{ref2}$, where

$$V_{ref2} = -2V_D - V_{DC} \tag{17}$$

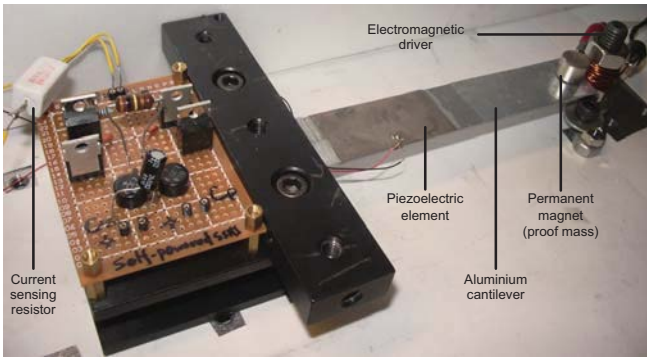

Fig. 7. Experimental setup.

is the second reference voltage gap, v_p will experience one more inversion. For the second inversion, i.e. from V_2 to V_3, C_p in series with C_{CE}, L and r form the LCR loop for discharging, with the quality factor of

$$Q_2 = \frac{1}{r}\sqrt{\frac{L(C_p + C_{CE})}{C_p C_{CE}}}. \tag{18}$$

The relation between V_3 and V_2 can be obtained as

$$V_3 - \frac{C_p}{C_{CE}}(V_2 - V_3) - V_{ref2} = \gamma_2(V_2 - V_{ref2}), \tag{19}$$

where

$$\gamma_2 = \begin{cases} -e^{-\pi/(2Q_2)}, & V_{1.5} < V_{ref2}; \\ 1, & \text{others} \end{cases} \tag{20}$$

is the inversion factor for the corresponding LCR loop, whose quality factor is Q_2.

The charge neutralization follows the second inversion. Since the resistor R_2 is used for slowing down the discharging process of C_2, roughly speaking, the time constant of R_2C_2 should be larger than τ, which was given in (11). So we can simply assume that the discharge of C_2 starts after the two inversion of v_p. In the charge neutralization, the total charge in C_p, C_1 and C_2 is unchanged. Considering their original voltage, V_4 is related to V_1, V_2 and V_3 with the following equation

$$(2C_{ed} + C_p)V_4 = C_{ed}(V_1 + V_2) + C_p V_3. \tag{21}$$

One more relation links V_1, V_4 and the open circuit voltage V_{OC}, i.e.

$$V_1 + V_4 = 2V_{OC}\cos\varphi. \tag{22}$$

$V_1 \sim V_4$ can be expressed in terms of V_{OC} and V_{DC} by solving the linear equations of (15), (19), (21) and (22).

Because of the complementary topology, for switching on minimum, the four corresponding voltages are $-V_1$, $-V_2$, $-V_3$, and $-V_4$, respectively.

D. Harvesting Power

Based on the above analyses about the influences of self-powered implementation to the open circuit voltage, switching phase lag and voltage inversion factor in SSHI, the analysis on harvesting power can be carried out.

In each vibration cycle, the harvested energy of the self-powered SSHI is

$$E_{SP-SSHI} = 2V_{DC}[C_p(V_1 + V_3 - 2V_2) + C_{ed}(V_1 - V_2)]. \tag{23}$$

Multiplying $E_{SP-SSHI}$ by the vibration frequency yields the harvesting power of the self-powered SSHI, as

$$P_{SP-SSHI} = f_0 E_{SP-SSHI}, \tag{24}$$

where $f_0 = \omega/(2\pi)$ is the vibration frequency.

Besides, for SEH and ideal SSHI[5], the harvesting powers are [6], [8]

$$P_{SEH} = 4f_0 C_p V_{DC}(V_{OC,org} - V_{DC} - 2V_D), \tag{25}$$

$$P_{SSHI} = 4f_0 C_p V_{DC}(V_{OC,org} - V_{DC} - 2V_D)\frac{1-\gamma}{1+\gamma}, \tag{26}$$

respectively.

TABLE I

CIRCUIT PARAMETERS.

Name	Symbol	Value
Diode forward voltage drop	V_D	0.5 V
Transistor base-emitter on voltage	V_{BE}	0.5 V
Transistor collector-emitter saturation voltage	$V_{CE(sat)}$	1.2 V [10]
Transistor emitter-collector capacitance	C_{CE}	150 pF [10]
Voltage inversion factor	γ_1	−0.52

V. EXPERIMENTS

Experiments are performed in order to evaluate the performance of practical self-powered SSHI. The experimental setup is shown in Fig. 7. It is built up with a piezoelectric cantilever and the modified self-power SSHI interface circuitry.

The main mechanical structure is an aluminium cantilever whose fixed end is fixed on the vibration-free table and the free end is driven by an electromagnetic driver. A piezoceramic patch of 49mm × 24mm × 0.508mm (T120-A4E-602, Piezo System, Inc.) is bonded near the fixed end where the largest strain happens along the cantilever. A permanent magnet is attached at the free end of the cantilever, so as to achieve the coupling with the electromagnetic driver; and it also acts as a proof mass to lower the vibration frequency and increase the displacement of the free end. A function generator (33120A, Agilent Co.), following by a power amplifier (2706, B&K Co.), provides a 30Hz sinusoidal excitation to the electromagnetic coil. To perform constant displacement excitation, an inductive displacement sensor (JCW-24SR, CNHF Co.), which is not shown in Fig. 7, is used to sense the displacement of the cantilever for adjustment under different situations.

For the circuitry, component models and values are the same as those shown in Fig. 4. Other circuit parameters are given in Table I.

[5]In ideal SSHI, the sensing and switching control units do not bring any V_{OC} influence, switching phase delay, and voltage gap to the circuit. However, the voltage gap of bridge rectifier is considered nonzero.

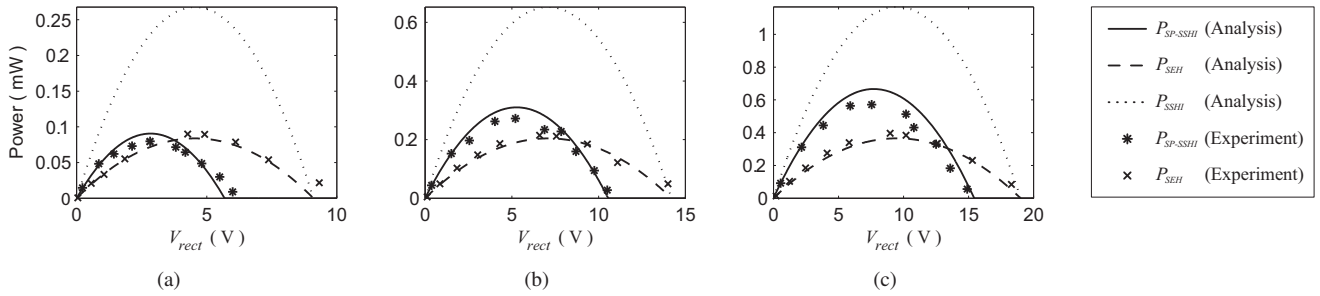

Fig. 8. Harvesting power under different excitation levels. (a) $V_{OC,org}$ = 10.1 V. (b) $V_{OC,org}$ = 15.2 V. (c) $V_{OC,org}$ = 20 V.

TABLE II

MEASURED CHANGES ON OPEN CIRCUIT VOLTAGE.

$V_{OC,org}$ (V)	V_{OC} (V)	$V_{OC}/V_{OC,org}$
10.1	9.7	0.9604
15.2	14.6	0.9605
20	9.2	0.9600

In experiments, firstly, the changes on open circuit voltage before and after the connection of self-powered SSHI circuit are checked under three excitation levels. As shown in Table II, the ratios of $V_{OC}/V_{OC,org}$ in these three situations agree with the ratio of $C_p/(C_p+2C_{ed}) = 0.9613$ in our experiment, which verified the analysis on open circuit voltage in Section IV.

Also under those three excitation levels, the harvesting power is measured as function of rectified voltage V_{DC}. Resistors with different resistance values are connected as loads one by one. With the corresponding measured DC voltage across each resistor, the harvesting power under different V_{DC} can be obtained. The experimental results of $P_{SP-SSHI}$ and P_{SEH} under three excitation levels, together with the analyzed $P_{SP-SSHI}$, P_{SEH} and P_{SSHI} are given in Fig. 8 for comparison.

From the three sub-figures in Fig. 8, both analytical and experimental results show good agreement with each other. Comparing the self-powered SSHI to the ideal SSHI, the higher the excitation level, the closer between $P_{SP-SSHI}$ and P_{SSHI}. On the other hand, comparing the self-powered SSHI to SEH, the maximum harvesting power in self-powered SSHI is larger than that in SEH only when the excitation level is high enough. Therefore, rather than claiming that self-powered SSHI always outperforms SEH, we should note that there should be a critical excitation level, below which this claim is unconvincing.

VI. CONCLUSION

The introduction of the self-powered version of synchronized switching harvesting on inductor (SSHI) treatment did open a promising territory for piezoelectric energy harvesting with switching technique. Nevertheless, many issues still lie in further improvements on both circuitry and precise modeling. We proposed a modified circuitry for self-powered SSHI. Compared to the circuitry proposed in [8], the modified circuitry not only minimize the interference among different units in the circuit, so as can enhance the switching performance; but also result in the removal of some resistive components, so as can further diminish the energy dissipation within the switching processes. Improved analysis was carried out considering three aspects of open circuit voltage, switching phase lag, and voltage inversion factor. Unlike the ideal SSHI, which always has better harvesting capability than SEH, it was found from both analyses and experiments that, for self-powered SSHI, only when the excitation level is high enough, it can outperform SEH. Moreover, the higher the excitation level, the more significant the enhancement on harvesting power; therefore, the more beneficial to replace the standard interface with such self-powered switching interface for piezoelectric energy harvesting.

ACKNOWLEDGMENT

The work described in this paper was supported by a grant from the Research Grants Council of the Hong Kong Special Administrative Region, China (Project No. CUHK4152/08E).

REFERENCES

[1] A. Ephremides, "Energy concerns in wireless networks," *IEEE Wirel. Commun.*, vol. 9, no. 4, pp. 48–59, Aug. 2002.

[2] J. Paradiso and T. Starner, "Energy scavenging for mobile and wireless electronics," *IEEE Pervasive Comput.*, vol. 4, no. 1, pp. 18–27, Jan.-March 2005.

[3] G. Ottman, H. Hofmann, A. Bhatt, and G. Lesieutre, "Adaptive piezoelectric energy harvesting circuit for wireless remote power supply," *IEEE Trans. Power Electron.*, vol. 17, no. 5, pp. 669–676, Sep 2002.

[4] G. Ottman, H. Hofmann, and G. Lesieutre, "Optimized piezoelectric energy harvesting circuit using step-down converter in discontinuous conduction mode," *IEEE Trans. Power Electron.*, vol. 18, no. 2, pp. 696–703, Mar 2003.

[5] D. Guyomar, A. Badel, E. Lefeuvre, and C. Richard, "Toward energy harvesting using active materials and conversion improvement by nonlinear processing," *IEEE Trans. Ultrason. Ferroelectr. Freq. Control*, vol. 52, no. 4, pp. 584–595, April 2005.

[6] E. Lefeuvre, A. Badel, C. Richard, L. Petit, and D. Guyomar, "A comparison between several vibration-powered piezoelectric generators for standalone systems," *Sens. Actuator A-Phys.*, vol. 126, no. 2, pp. 405 – 416, 2006.

[7] K. Makihara, J. Onoda, and T. Miyakawa, "Low energy dissipation electric circuit for energy harvesting," *Smart Mater. Struct.*, vol. 15, no. 5, pp. 1493–1498, 2006.

[8] M. Lallart and D. Guyomar, "An optimized self-powered switching circuit for non-linear energy harvesting with low voltage output," *Smart Mater. Struct.*, vol. 17, no. 3, p. 035030 (8pp), 2008.

[9] J. R. Liang and W. H. Liao, "Piezoelectric energy harvesting and dissipation on structural damping," *J. Intell. Mater. Syst. Struct.*, vol. 20, no. 5, pp. 515–527, 2009.

[10] *TIP31C and TIP32C Datasheet*, ON Semiconductor, Dec. 2008.